Oligomerization Versus Polymerization of Te_x^{n-} in the Polytelluride Compound $BaBiTe_3$. Structural Characterization, Electronic Structure, and Thermoelectric Properties

Duck-Young Chung,[†] Stéphane Jobic,[‡] Tim Hogan,[§,#] Carl R. Kannewurf,[§] Raymond Brec,[‡] Jean Rouxel,[‡] and Mercouri G. Kanatzidis*[,†,‡]

Contribution from the Department of Chemistry and Center for Fundamental Materials Research, Michigan State University, East Lansing, Michigan 48824, Institut des Matériaux de Nantes, 2 Rue de la Houssinière, 44072 Nantes Cedex 03, France, and Department of Electrical Engineering and Computer Science, Northwestern University, Evanston, Illinois 60208

Received October 18, 1996. Revised Manuscript Received January 6, 1997[⊗]

Abstract: The compound $BaBiTe_3$ was prepared by the reaction of Ba/Bi/Te at over 700 °C in either K_2Te_4 or $BaTe_3$ flux and was recrystallized in a $Ba/BaTe_3$ flux. The black rod-shaped polycrystalline material crystallizes in the orthorhombic space group $P2_12_12_1$ (no. 19) with $a = 4.6077(2)$ Å, $b = 17.0437(8)$ Å, $c = 18.2997(8)$ Å, $V = 1437.1(2)$ Å^3, $Z = 8$, and $d_{calc} = 6.74$ g/cm^3. Number with $F_o^2 > 3\sigma(F_o)^2$ 3373, number of variables 92, and sin $(\theta/\lambda) < 0.7$. The final $R/R_w = 4.55/5.61\%$. The structure is $BaBiSe_3$ type and may be described as layers made up from interdigitating columnar $[Bi_4Te_{10}(Te_2)]_\infty$ "herring-bone" shaped segments. Ba^{2+} ions are in distorted tri-capped trigonal prismatic sites between the layers. From band structure calculations, a formal charge distribution taking into account the occurrence of short-bonding Te···Te contacts in the structure can be written as $Ba^{2+}{}_4Bi^{3+}{}_4Te^{2-}{}_8Te^{1-}{}_4$. The electrical conductivity, thermopower, thermal lattice conductivity, and infrared absorption properties of this material suggest that it is a narrow gap semiconductor. These results are discussed in the context of the band scheme.

Introduction

Interest in Group 15 chalcogenides is increasing because such materials may possess enhanced thermoelectric properties.[1] Bi_2Te_3 and its solid solutions[2] are currently the leading thermoelectric materials for room temperature cooling applications. This reflects the fact that this material exhibits the unusual combination of simultaneously high electrical conductivity, high thermoelectric power, and low thermal conductivity. The origin of this phenomenon is not entirely understood. In most materials high electrical conductivity is characterized by low thermoelectric power and vice versa. Therefore, it is difficult to come up with a robust theoretical framework to search for new thermoelectric materials. Nevertheless, new materials incorporating bismuth have not been extensively explored during the past three decades, and thus we have embarked in a chemically based approach to prepare and study the properties of structural and chemical derivatives of Bi_2Q_3 (Q = S, Se, Te). The variation in properties of such materials could reveal interesting trends from which we could benefit in constructing better theoretical frameworks for understanding and designing efficient thermoelectric materials. Recently, several new ternary alkali metal Group 15 chalcogenides were synthesized such as $KBi_{6.33}S_{10}$,[3] $K_2Bi_8Q_{13}$ (Q = S, Se),[3,4] ABi_3S_5 (A = K, Rb, Cs),[5−7] $RbBiQ_2$ (Q = S, Se),[8] β-,γ-$CsBiS_2$,[4] and $Cs_3Bi_7Se_{12}$.[9] Past exploratory work in bismuth telluride compounds has concentrated on introducing a heavy metal into a binary Bi/Te system to give ternary phases such as in $PbBi_2Te_4$,[10−12] $Pb_2Bi_2Te_5$,[12,14] $PbBi_4Te_7$,[11−13] $Pb_9Bi_2Te_{12}$,[11] $TlBiTe_2$,[15] $TlBiTe_3$,[16] $TlBi_2Te_3$,[17] Tl_9BiTe_6,[18] $SbBiTe_2$,[19] $SbBiTe_3$,[20] $Sb_2Bi_2Te_3$,[19] and $Sb_8Bi_2Te_{15}$.[19] With the exception of $ABiTe_2$ (A = Li, Na, K, Rb,

[†] Michigan State University.
[‡] Institut des Materiaux de Nantes.
[§] Northwestern University.
[#] Current address: Department of Physics, University of Houston, Houston, TX 77204-5506.
[⊗] Abstract published in *Advance ACS Abstracts,* February 15, 1997.

(1) (a) *CRC Handbook of Thermoelectrics*; Rowe, D. M., Ed.; CRC Press, Inc.: Boca Raton, FL, 1995. (b) Kaibe, H.; Tanaka, Y.; Sakata, M.; Nishida, I. *J. Phys. Chem. Solids* **1989**, *50*, 945−950. (c) Jeon, H.-H.; Ha, H.-P.; Hyun, D.-B.; Shim, J.-D. *J. Phys. Chem. Solids* **1991**, *4*, 579−585.
(2) (a) Testardi, L. R.; Bierly, J. N., Jr.; Donahoe, F. J. *J. Phys. Chem. Solids* **1962**, *23*, 1209. (b) Champness, C. H.; Chiang, P. T.; Parekh, P. *Can. J. Phys.* **1965**, *43*, 653−659. (c) Yim, W. M.; Fitzke, E. V. *J. Electrochem. Soc.* **1968**, *115*, 556−560.
(3) Kanatzidis, M. G.; McCarthy, T. J.; Tanzer, T. A.; Chen, L.-H.; Iordanidis, L.; Hogan, T.; Kannewurf, C. R.; Uher, C.; Chen, B. *Chem. Mater.* **1996**, *8*, 1465−1474.
(4) McCarthy, T. J.; Ngeyi, S.-P.; Liao, J.-H.; DeGroot, D. C.; Hogan, T.; Kannewurf, C. R.; Kanatzidis, M. G. *Chem. Mater.* **1993**, *5*, 331−340.
(5) McCarthy, T. J.; Tanzer, T. A.; Kanatzidis, M. G. *J. Am. Chem. Soc.* **1995**, *117*, 1294−1301.
(6) Schmitz, D.; Bronger, W. Z. *Z. Naturforsch.* **1974**, *29b*, 438−439.
(7) Kanischcheva, A. S.; Mikhailov, J. N.; Lazarev, V. B.; Trippel, A. F. *Dokl. Akad. Nauk. SSSR (Krist.)* **1980**, *252*, 96−99.
(8) Voroshilov, Y. V.; Peresh, E. Y.; Golovei, M. I. *Inorg. Mater.* **1972**, *8*, 777−778.
(9) Cordier, G.; Schäfer, H.; Schwidetzky, C. *Rev. Chim. Miner.* **1985**, *22*, 676−683.
(10) Zhukova, T. B.; Zaslavskii, A. I. *Sov. Phys. Crystallogr.* **1971**, *16*, 796−800.
(11) Chami, R.; Brun, G.; Tedenac, J.-C. *Rev. Chim. Miner.* **1983**, *20*, 305−313.
(12) Zhukova, T. B.; Zaslavskii, A. I. *Inorg. Mater.* **1976**, *12*, 467−469.
(13) (a) Golovanova, N. S.; Zlomanov, V. P.; Tananaeva, O. I. *Inorg. Mater.* **1983**, *19*, 669−672. (b) Abrikosov, N. Kh.; Skudnova, E. V.; Poretskaya, L. V.; Osipova, T. A. *Inorg. Mater.* **1970**, *10*, 1424−1427. (c) Frumer, M.; Horák, J. *J. Phys. Status Solidi A* **1971**, *6*, k133−k137.
(14) Petrov, I. I.; Imamov, R. M. *Sov. Phys. Crystallogr.* **1969**, *14*, 593−596.
(15) (a) Hockings, E. F.; White, J. G. *Acta Crystallogr.* **1961**, *14*, 328. (b) Marin, R. M.; Abdelhady, D.; Tedenac, J. C.; Maurin, M.; Brun, G. *Mater. Res. Bull.* **1987**, *22*, 149−155.
(16) Borisova, L. A.; Efremova, M. V.; Vlasov, V. V. *Dokl. Akad. Nauk. SSSR* **1963**, *149*, 117−119.
(17) Borisova, L. A.; Efremova, M. V.; Akhmedova, F. I. *Russ. J. Inorg. Chem.* **1963**, *8*, 1415−1418.
(18) Voroshilov, Yu. V.; Gurzan, M. I.; Kish, Z. Z.; Lada, L. V. *Inorg. Mater.* **1988**, *24*, 1266−1269.

S0002-7863(96)03649-9 CCC: $14.00

Cs)[21] and the Zintl phase $K_3[BiTe_3]$,[22] few phases have been prepared with alkali or alkaline earth metals in the ternary bismuth telluride system. One of the challenges in this chemistry is the high stability of Bi_2Te_3 in the temperature range from 200 to 800 °C.

In this work we have examined the Ba/Bi/Te system in detail and report on the synthesis, structure, infrared absorption properties, electrical conductivity, and thermoelectric power of $BaBiTe_3$. We also report thermal conductivity measurements which show that this material has one of the lowest κ_L (lattice thermal conductivity) values known for crystalline metal chalcogenides. Extended Hückel and LMTO band structure calculations were also carried out to probe the Te−Te interactions observed in this compound and to get a deeper insight of the electronic structure near the Fermi level and the electrical properties of $BaBiTe_3$.

Experimental Section

Reagents. Chemicals in this work were used as obtained: (i) bismuth powder, 99.999+% purity, −100 mesh, Cerac, Milwaukee, WI, (ii) tellurium powder, 99.95%, −200 mesh, Johnson Matthey/AESAR Group, Seabrook, NH; and (iii) barium metal, granules, <6 mm, 99% purity, Aldrich Chemical Co., Inc., Milwaukee, WI.

Synthesis. All manipulations were carried out under a dry nitrogen atmosphere in a Vacuum Atmospheres Dri-Lab glovebox. Crystals of $BaBiTe_3$ could be obtained with Ba/Bi/Te/K_2Te_4 or Bi/$BaTe_3$ flux reactions.

$BaTe_3$. A mixture of 13.94 g (0.11 mol) of Te and 5 g (0.036 mol) of Ba metal of granule type was added to a 250-mL, round-bottom flask. A 150-mL volume of liquid NH_3 was condensed into a round-bottom flask at −78 °C (dry ice/acetone) under nitrogen to give a dark reddish brown solution. The solution was stirred overnight and the NH_3 was removed by evaporation under a flow of nitrogen as the bath slowly warmed to room temperature. The black solid was dried under vacuum overnight and ground to a fine powder. Great care was taken to avoid exposure of the product to air.

Better crystallized $BaTe_3$ could be prepared by the stoichiometric reaction of elemental Ba and Te at 550 °C.[23]

$BaBiTe_3$. Method I. A mixture of 0.439 g (0.75 mmol) of K_2Te_4, 0.103 g (0.75 mmol) of Ba, 0.104 g (0.5 mmol) of Bi, and 0.096 g (0.75 mmol) of Te was loaded into a carbon-coated 6-mL quartz tube. The tube was evacuated to a residual pressure of $<10^{-4}$ Torr and flamed-sealed. The mixture was heated to 750 °C over 24 h and kept at that temperature for 4 days followed by a slow cooling (4 °C/h) to 200 °C. The product was isolated by removing the excess flux with degassed dimethylformamide and water under a nitrogen atmosphere. Black rods of $BaBiTe_3$ mixed with Bi_2Te_3 were obtained in approximately 50% yield based on Bi. This mixed phase product can be recrystallized in a K_2Te_x/BaTe flux at 720 °C (3.5 days, cooling at 4 °C/h) to yield single crystals of p-type $BaBiTe_3$.

Method II. A mixture of 0.377 g (0.96 mmol) of Cs_2Te, 0.066 g (0.48 mmol) of Ba, 0.1 g (0.48 mmol) of Bi, and 0.489 g (3.83 mmol) of Te was loaded into a carbon-coated 6-mL quartz tube and heated at 600 °C for 4 days. After cooling to 200 °C at a rate of 4 °C/h, the product which gave an 80% yield of large rods of $BaBiTe_3$ and 20% plates of Bi_2Te_3 was isolated as above. EDS analysis showed no Cs in the compound. This procedure yields n-type material.

Method III. A mixture of 1.120 g (2.2 mmol) of $BaTe_3$ and 0.150 g (0.72 mmol) of Bi in a carbon-coated quartz tube was heated at 700 °C for 5 days. After the mixture was cooled to 150 °C at a rate of 4 °C/h, the product was isolated as above. The yield of $BaBiTe_3$ was approximately 60% based on Bi. A small amount of Bi_2Te_3 impurity was present in this sample as well. A quantitative microprobe analysis with a SEM/EDS system was performed on several crystals from both methods and gave an average ratio of $Ba_{0.8}Bi_{1.1}Te_3$.

Recrystallization and Single Crystal Growth. A 0.35-g sample of raw product isolated above was ground to fine powder and mixed with 0.093 g (0.68 mmol) of Ba and 0.464 g (0.89 mmol) of $BaTe_3$. After the mixture was loaded into an alumina thimble (9.5 mm o.d. × 6.5 mm i.d. × 75 mm) it was sealed inside a quartz tube (13 mm o.d. × 11 mm i.d.). The tube was slowly heated to 750 °C over 2 days and kept there for 3 days to complete the recrystallization process. It was then slow cooled at the rate of 4 °C/h to 150 °C. The relatively large crystals (>1 mm) were isolated in degassed water and the purity of the $BaBiTe_3$ phase was checked by Differential Thermal Analysis (DTA) and X-ray powder diffraction (XRD). There was no sign of any impurities including Bi_2Te_3.

Physical Measurements. (a) Electron Microscopy. Quantitative microprobe analyses of the compound were performed with a JEOL JSM-35C Scanning Electron Microscope (SEM) equipped with a Tracor Northern Energy Dispersive Spectroscopy (EDS) detector. Data were acquired using an accelerating voltage of 20 kV and a 1 min accumulation time.

(b) Differential Thermal Analysis. Differential Thermal Analysis (DTA) was performed with a computer-controlled Shimadzu DTA-50 thermal analyzer. The ground single crystals (~20 mg total mass) were sealed in quartz ampules under vacuum. A quartz ampule containing alumina of equal mass was sealed and placed on the reference side of the detector. The samples were heated to the desired temperature at 10 °C/min, then isothermed for 3 min followed by cooling at 10 °C/min to 100 °C and finally by rapid cooling to room temperature. The reported DTA temperature is the peak temperature. The DTA sample was examined by powder X-ray diffraction after the experiment.

(c) Infrared Spectroscopy. Optical diffuse reflectance measurements were made on the finely ground sample at room temperature. The spectrum was recorded in the infrared region (6000−400 cm^{-1}) with the use of a Nicolet MAGNA-IR 750 Spectrometer equipped with a Collector Diffuse Reflectance of Spectra-Tech. Inc. The measurement of diffuse reflectivity can be used to obtain values for the band gap which agree rather well with the values obtained by absorption measurements from single crystals of the same material. Absorption (α/S) data were calculated from the reflectance data using the Kubelka−Munk function.[24] The band gap was determined as the intersection point between energy axis at the absorption offset and the line extrapolated from the linear portion of the absorption edge in a α/S vs E plot.

(d) Charge-Transport and Thermal Conductivity Measurements. DC electric conductivity and thermopower measurements were made on single crystals and polycrystalline compactions of the compound. Conductivity measurements were performed in the usual four-probe geometry with 60- and 25-μm gold wires used for the current and voltage electrodes, respectively. Measurements of the pellet cross-sectional area and voltage probe separation were made with a calibrated binocular microscope. Conductivity data were obtained with the computer-automated system described elsewhere.[25a] Thermoelectric power measurements were made by using a slow ac technique[25b] with 60-μm gold wires serving to support and conduct heat to the sample, as well as to measure the voltage across the sample resulting from the applied temperature gradient. In both measurements, the gold electrodes were held in place on the sample with a conductive gold paste.

Conductivity specimens were mounted on interchangeable sample holders, and thermopower specimens were mounted on a fixed sample holder/differential heater. Mounted samples were placed under vacuum (10^{-3} Torr) and heated to room temperature for 2−4 h to cure the gold contacts. For a variable-temperature run, data (conductivity or thermopower) were acquired during both sample cooling and warming to

(19) Stasova, M. M.; Abrikosov, N. Kh. *Inorg. Mater.* **1970**, *6*, 953−956.
(20) Smith, M. J.; Knight, R. J.; Spencer, C. W. *J. Appl. Phys.* **1962**, *33*, 2186−2190.
(21) Eisenmann, V. B.; Schäfer, H. *Z. Anorg. Allg. Chem.* **1979**, *456*, 87−94.
(22) Eisenmann, B.; Zagler, R. *Z. Kristallogr.* **1991**, *197*, 257−258.
(23) Cordier, G.; Shwidetaky, C.; Schäfer, H. *Z. Naturforsch.* **1984**, *39B*, 833−834.
(24) (a) Wendlandt, W. W.; Hecht, H. G. *Reflectance Spectroscopy*; Interscience Publishers: New York, 1966. (b) Kotüm, G. *Reflectance Spectroscopy*; Springer-Verlag: New York, 1969. (c) Tandon, S. P.; Gupta, J. P. *Phys. Status Solidi* **1970**, *38*, 363−367.
(25) (a) Lyding, J. W.; Marcy, H. O.; Marks, T. J.; Kannewurf, C. R. *IEEE Trans. Instrum. Meas.* **1988**, *37*, 76−80. (b) Chaikin, P. I.; Kawk, J. F. *Rev. Sci. Instrum.* **1975**, *46*, 218−220.

check reversibility. The temperature drift rate during an experiment was kept below 1 K/min. Typically, three to four separate variable-temperature runs were carried out for each sample to ensure reproducibility and stability. At a given temperature, reproducibility was within ±5%.

Thermal conductivity measurements were taken using a pulse technique in a computer-controlled system. The technique described by Maldonado was modified to incorporate a four probe measurement configuration.[26] In this measurement, both thermal conductivity and thermoelectric power are simultaneously measured. For comparison, thermoelectric power measurements were also taken in a separate measurement system using the slow-ac technique mentioned above and showed good agreement with results from the pulse technique.

(e) Crystallography. The compound was examined by X-ray powder diffraction for the purpose of phase purity and identification (see Table 1). Accurate unit cell parameters were determined by a least-squares refinement from data collected on a CPS 120 INEL X-ray powder diffractometer using monochromatized radiation Cu K-L_{III} (λ = 1.54059 Å) and equipped with a position-sensitive detector calibrated with $Na_2Ca_3Al_2F_{14}$ as standard.[28] The refinement of the diagram in the 16−114° 2θ range yields a = 4.6077(2) Å, b = 17.0437(8) Å, and c = 18.2997(8) Å.

A single crystal of $BaBiTe_3$ with dimensions 0.03 × 0.06 × 0.52 mm was mounted on the tip of a glass fiber. The crystallographic data were collected at room temperature on a Siemens P4 diffractometer (Euler geometry, Ag K-$L_{II,III}$ radiation, and graphite monochromator). Ag K-$L_{II,III}$ radiation was used to minimize the absorption correction problem. The intensities of three standard reflections were checked every 100 reflections to monitor crystal and instrument stability. No significant decay was observed during the data collection period. The data were collected with the omega scan technique. The unit cell parameters were determined from a least-squares refinement using the setting angles of 28 carefully centered reflections in the $9 \le 2\theta \le 25°$ range. The structure was solved by direct methods using the SHELXS-86[29] software program. After Gaussian-type absorption corrections and averaging of equivalent reflections, refinements with full-matrix least-squares techniques and Fourier synthesis calculations were carried out with the SDS program.[30] All atoms were refined anisotropically. Table 2 shows the crystal data and the details of the structure analysis. The fractional coordinates and the equivalent atomic displacement parameters (B_{eq}) of all the atoms with their estimated standard deviations are given in Table 3. Selected bond lengths and angles in the compound are summarized in Tables 4 and 5.

(f) Electronic Structure Calculations. The charge balance and the nature of the internal redox competition between $[Bi_4Te_{10}]$ rods and would-be $[Te_2]$ "chains" were probed with tight-binding band structure calculations[31] using an extended Hückel-type Hamiltonian.[32] A modified Wolfsberg−Helmholz formula was used to calculate the non-diagonal H_{ij} values.[33] The ionization potentials (eV) and exponents used were the following: −15.19 and 2.56 for Bi 6s, −7.79 and 2.072 for Bi 6p,[34] −20.78 and 2.51 for Te 5s, and −13.20 and 2.16 for Te 5p.[35] Although the results of these calculations depend on the initial H_{ii} parameters, we found that variations of these parameters did not qualitatively affect the interpretation of the final results. Calculations on a $[Bi_4Te_{12}]_n^{8n-}$ sheet were performed with a 100 k-point grid in the irreducible first Brillouin zone. A k-point mesh of 60 was used for the $[Bi_4Te_{10}]_n$ rods and $[Te_2]_n$ "chains". The calculations were performed without taking into account Ba atomic orbitals. In effect, Ba is much more electropositive than Bi and Te (χ_{Ba} = 0.89, χ_{Bi} = 2.02, χ_{Te} = 2.10 according to the Pauling electronegativity scale), and

Table 1. Observed and Calculated d Spacings (Å) for $BaBiTe_3$ Determined from the Lazy Pulverix Program,[27] and Observed Intensities

h	k	l	d_{calc}	d_{obsd}	I_{obsd}
0	1	1	12.47	12.47	6.59
0	0	2	9.15	9.15	1.46
0	2	0	8.52	8.53	6.73
0	1	2	8.06	8.07	1.46
0	2	1	7.73	7.74	2.05
0	2	2	6.24	6.23	3.51
0	3	1	5.43	5.42	3.37
0	2	3	4.96	4.96	4.39
0	3	2	4.83	4.82	3.22
0	1	4	4.419	4.415	5.12
1	1	1	4.322	4.320	3.81
0	3	3	4.157	4.156	10.10
1	2	1	3.958	3.964	6.73
0	4	2	3.862	3.861	10.40
1	1	3	3.594	3.598	23.57
0	5	1	3.351	3.357	28.55
1	0	4	3.247	3.249	11.27
1	1	4	3.189	3.192	100
1	3	3	3.087	3.088	13.47
1	2	4	3.034	3.036	45.68
0	5	3	2.976	2.975	4.69
1	1	5	2.826	2.828	3.66
0	4	5	2.776	2.776	4.54
1	5	2	2.625	2.626	5.56
1	3	5	2.559	2.560	13.76
1	2	6	2.437	2.437	3.51
1	4	5	2.378	2.379	5.86
1	6	2	2.338	2.339	5.27
2	0	0	2.304	2.309	11.71
0	5	6	2.273	2.271	3.51
1	6	3	2.248	2.252	19.77
0	2	8	2.209	2.210	3.66
1	4	6	2.184	2.184	15.67
0	3	8	2.122	2.119	5.56
1	7	2	2.096	2.097	9.37
0	8	2	2.075	2.076	5.27
0	1	9	2.019	2.020	4.98
0	2	9	1.978	1.977	5.12
2	0	5	1.950	1.951	2.05
1	3	8	1.927	1.924	3.51
0	7	6	1.903	1.902	6.88
2	5	2	1.869	1.872	6.15
1	7	5	1.856	1.856	2.93
1	8	3	1.843	1.843	2.78
0	7	7	1.782	1.784	3.07
0	9	4	1.750	1.750	3.22
1	9	2	1.720	1.723	1.90
2	2	7	1.694	1.693	11.57
1	2	10	1.668	1.668	2.49
0	6	9	1.653	1.653	2.34
1	9	4	1.636	1.635	3.51
0	9	6	1.609	1.610	3.66
2	2	8	1.595	1.596	6.59
1	10	2	1.575	1.573	12.59

(26) Maldonado, O. *Cryogenics* **1992**, *32*, 908−912.
(27) Yvon, R.; Jeitschko, W.; Parthé, E. *J. Appl. Crystallogr.* **1977**, *10*, 73−74.
(28) (a) Deniard, P.; Evain, M.; Barbet, J. M.; Brec, R. *Mater. Sci. Forum* **1991**, *79*−82, 363−370. (b) Evain, M.; Deniard, P.; Jouanneaux, A.; Brec, R. *J. Appl. Crystallogr.* **1993**, *26*, 563−569.
(29) Sheldrick, G. M. *Crystallographic Computing 3*; Sheldrick, G. M., Kruger, C., Doddard, R., Eds.; Oxford University Press: Oxford, England, 1985; pp 175−189.
(30) (a) Petricek, V. *SDS 94*; Institute of Physics: Praha, Czech Republic, 1994. (b) There is no particular problem when the very high angle data are included except that the residues are somewhat high: +6.8 and 7.2 e/Å^3, the former being found at x = 0.234, y = 0.876, and z = 0.071, the latter at x = 0.265, y = 0.089, and z = 0.531. The intensities of these residues decrease substantially to +5.47 and −5.82 e/Å^3 after exclusion of the high angle data and the reliability factors drop from R = 4.98% and R_w = 5.87% to R = 4.55% and R_w = 5.61%. These results were found more satisfactory because they leave the atomic positional parameters unchanged while maintaining a fair number of data/number of variable ratio. Most likely, the high residues stem from absorption problems (Ba, Bi, and Te are heavily absorbing elements). Low-temperature data collection would not help much in this case.
(31) Whangbo, M.-H.; Hoffman, R. *J. Am. Chem. Soc.* **1978**, *100*, 6093−6098.
(32) Hoffmann, R. *J. Chem. Phys.* **1963**, *39*, 1397−1412.
(33) Ammeter, J. H.; Bürgi, H.-B.; Thibeault, J.; Hoffmann, R. *J. Am. Chem. Soc.* **1978**, *100*, 3686−3692.
(34) Lohr, L. L.; Pykko, P. *Chem. Phys. Lett.* **1979**, *62*, 333−338.
(35) Canadell, E.; Whangbo, M.-H. *Inorg. Chem.* **1990**, *29*, 1398−1401.

Table 2. Summary of Crystallographic Data for $BaBiTe_3$

empirical formula	$BaBiTe_3$
formula wt	729.110 g
crystal habit	black rod
crystal size	$0.03 \times 0.06 \times 0.52$ mm^3
space group	$P2_12_12_1$ (no. 19)
a[a]	4.6077(2) [4.626(1)] Å
b[a]	17.0437(8) [17.070(2)] Å
c[a]	18.2997(8) [18.320(4)] Å
volume	1437.1(2) Å^3
formula units per cell	$Z = 8$
calcd density	6.74 g/cm^{-3}
temperature	298 K
radiation, λ(Ag K-$L_{II,III}$)	0.56087 Å
linear absorption, μ(Ag Kα)	111.18 cm^{-1}
scan mode	ω
2θ range for data collection	2.0−54.0°
hkl range	$-1 \le h \le 7$, $-1 \le k \le 27$, $-29 \le l \le 29$
absorption correction	Gaussian method
total recorded reflcns	8979
independent reflcns with $I > 3\sigma(I)$	4543
independent reflcns with $I > 3\sigma(I)$ and $\sin(\theta/\lambda) < 0.7$[b]	3373
no. of refined parameters	92
final R[c]/R_w[d]	4.55/5.61%
goodness of fit	1.42
diff Fourier max and min peak intensity	5.47, −5.82 e$^-$/Å^3

[a] Values in brackets are determined from the single crystal measurements. [b] See ref 30b. [c] $R = \sum(|F_o| - |F_c|)/\sum|F_o|$. [d] $R_w = (\sum w(|F_o| - |F_c|)^2/\sum w|F_o|^2)^{1/2}$.

Table 3. Fractional Atomic Coordinates and Equivalent Atomic Displacement Parameter (B_{eq}) Values for $BaBiTe_3$ with Estimated Standard Deviations in Parentheses

atom	x	y	z	B_{eq},[a] Å^2
Bi(1)	0.2731(2)	0.21721(4)	0.29794(3)	1.64(2)
Bi(2)	−0.2382(2)	0.36949(4)	0.46806(4)	1.58(2)
Ba(1)	0.2334(3)	0.60527(6)	0.40411(5)	1.24(2)
Ba(2)	0.2439(3)	0.46063(6)	0.16501(6)	1.50(2)
Te(1)	0.2384(4)	0.40075(6)	0.36362(6)	1.40(2)
Te(2)	0.2601(4)	0.06173(6)	0.22940(6)	1.28(2)
Te(3)	0.7296(3)	0.17490(7)	0.40677(6)	1.54(2)
Te(4)	−0.2570(3)	0.53002(6)	0.52536(6)	1.27(2)
Te(5)	0.2066(3)	0.20792(7)	0.81008(6)	1.53(2)
Te(6)	0.2982(3)	0.26416(7)	0.05800(7)	1.95(2)

[a] Anisotropically refined atoms are given in the form of the isotropic equivalent displacement parameter defined as $B_{eq} = (8\pi^2/3)[a^2B_{11} + b^2B_{22} + c^2B_{33} + ab(\cos\gamma)B_{12} + ac(\cos\beta)B_{13} + bc(\cos\alpha)B_{23}]$. The anisotropic temperature factor expression is $\exp[-2\pi^2(B_{11}a^{*2}h^2 + ... + 2B_{12}a^*b^*hk + ...)]$.

it can reasonably be assumed that it provides 2e$^-$ per atom to the Bi/Te framework. Ba acts thus essentially as an electron donor and $BaBiTe_3$ can be considered as a Zintl phase.

Results and Discussion

Synthesis and Thermal Analysis. The known $BaSbQ_3$ (Q = Se, Te) and $BaBiSe_3$ were synthesized by direct combination of a mixture of elements or alkaline earth metal acetate with Group 15 metal and elemental chalcogen.[36] In contrast, K_2Te_4, $BaTe_3$, and Cs_2Te_x were adopted in this work as the reaction media. The flux reaction is particularly useful in growing single crystals and stabilizing structural fragments which are not stable at high temperature.[37] During our studies with alkali metal polytelluride fluxes, we noticed that potassium metal was rarely incorporated in most reactions with the Bi/Te system in temperatures between 400 and 800 °C. Thus, K_2Te_4 was first examined as an effective reaction medium in this research. The $BaTe_3$ flux improved slightly the yield and size of the crystals, compared to the K_2Te_4 flux, but a very slow and stepwise heating process was necessary due to a violent exothermic reaction starting at 300 °C. $BaBiTe_3$ was also prepared at high yield by using a Cs_2Te_x flux. From these synthetic experiments, we found that Ba, rather than akali metal, incorporates the Bi/Te system even in high concentration of the akali metal polytelluride flux. A byproduct was identified to be Bi_2Te_3 by X-ray powder diffraction analysis. Pure $BaBiTe_3$ was obtained in a Ba/$BaTe_3$ flux at 750 °C by recrystallizing the raw product isolated. The reaction using direct combination of the elements at slightly below 800 °C gave silvery white agglomerates of a microcrystalline mixture of $BaBiTe_3$ and Bi_2Te_3.

Differential Thermal Analysis (DTA) experiments performed on $BaBiTe_3$ showed that the compound undergoes slow decomposition when brought to melting at 643.5 °C. X-ray powder diffraction analysis of the residue material showed peritectic decomposition to Bi_2Te_3 and an unknown product, presumably a barium polytelluride melting at 455.8 °C.

Structure Description. The structure of $BaBiTe_3$ is layered

Table 4. Selected Distances (Å) in $BaBiTe_3$ with Standard Deviations in Parentheses[a]

Bi(1)−Te(1)	3.355(1)	Bi(2)−Te(1)	2.960(2)
Bi(1)−Te(2)	2.933(1)	Bi(2)−Te(1)	3.123(2)
Bi(1)−Te(3)	2.985(2)	Bi(2)−Te(3)	3.235(2)
Bi(1)−Te(3)	3.280(2)	Bi(2)−Te(3)	3.440(2)
Bi(1)−Te(5)	3.087(2)	Bi(2)−Te(3)	3.504(1)
Bi(1)−Te(5)	3.514(2)	Bi(2)−Te(4)	2.931(1)
Te(5)−Te(6)	3.098(2)	Te(6)−Te(6)	3.170(2)
Te(5)−Te(6)	3.672(2)		
Ba(1)−Te(1)	3.564(1)	Ba(2)−Te(1)	3.775(2)
Ba(1)−Te(2)	3.419(2)	Ba(2)−Te(2)	3.453(2)
Ba(1)−Te(2)	3.459(2)	Ba(2)−Te(2)	3.478(2)
Ba(1)−Te(4)	3.417(2)	Ba(2)−Te(3)	3.883(2)
Ba(1)−Te(4)	3.476(2)	Ba(2)−Te(4)	3.404(2)
Ba(1)−Te(5)	3.630(2)	Ba(2)−Te(4)	3.485(2)
Ba(1)−Te(6)	3.531(2)	Ba(2)−Te(5)	3.606(2)
Ba(1)−Te(6)	3.592(2)	Ba(2)−Te(5)	3.820(2)
Ba(1)−Te(6)	3.717(2)	Ba(2)−Te(6)	3.887(2)

[a] Calculated using the cell parameters refined from the powder X-ray diffraction diagram.

Table 5. Selected Angles (deg) in $BaBiTe_3$ with Standard Deviations in Parentheses[a]

Te(1)−Bi(1)−Te(2)	174.19(5)	Te(1)−Bi(2)−Te(1)	98.46(4)
Te(1)−Bi(1)−Te(3)	91.14(4)	Te(1)−Bi(2)−Te(3)	171.04(4)
Te(1)−Bi(1)−Te(3)	87.20(4)	Te(1)−Bi(2)−Te(3)	176.93(4)
Te(1)−Bi(1)−Te(5)	82.81(4)	Te(1)−Bi(2)−Te(3)	90.27(4)
Te(1)−Bi(1)−Te(5)	80.07(4)	Te(1)−Bi(2)−Te(3)	89.71(4)
Te(2)−Bi(1)−Te(3)	94.67(4)	Te(1)−Bi(2)−Te(3)	83.96(4)
Te(2)−Bi(1)−Te(3)	92.60(4)	Te(1)−Bi(2)−Te(3)	86.16(3)
Te(2)−Bi(1)−Te(5)	96.48(4)	Te(1)−Bi(2)−Te(4)	92.12(4)
Te(2)−Bi(1)−Te(5)	94.15(4)	Te(1)−Bi(2)−Te(4)	94.87(4)
Te(3)−Bi(1)−Te(3)	94.58(4)	Te(3)−Bi(2)−Te(3)	87.25(4)
Te(3)−Bi(1)−Te(5)	170.55(4)	Te(3)−Bi(2)−Te(3)	91.92(3)
Te(3)−Bi(1)−Te(5)	94.08(4)	Te(3)−Bi(2)−Te(3)	88.56(3)
Te(3)−Bi(1)−Te(5)	81.62(4)	Te(3)−Bi(2)−Te(4)	175.30(5)
Te(3)−Bi(1)−Te(6)	166.89(4)	Te(3)−Bi(2)−Te(4)	89.12(4)
Te(5)−Bi(1)−Te(5)	88.30(4)	Te(3)−Bi(2)−Te(4)	86.91(4)
Bi(1)−Te(1)−Bi(2)	95.67(4)	Bi(1)−Te(3)−Bi(2)	93.40(5)
Bi(1)−Te(1)−Bi(2)	91.34(4)	Bi(1)−Te(3)−Bi(2)	90.84(4)
Bi(2)−Te(1)−Bi(2)	98.46(4)	Bi(1)−Te(3)−Bi(2)	178.68(5)
Bi(1)−Te(5)−Te(6)	92.43(5)	Bi(1)−Te(3)−Bi(2)	171.93(5)
Bi(1)−Te(5)−Te(6)	146.49(5)	Bi(2)−Te(3)−Bi(2)	91.31(3)
Te(5)−Te(6)−Te(6)	95.96(6)	Bi(2)−Te(3)−Bi(2)	87.99(3)
Te(5)−Te(6)−Te(6)	170.70(7)	Bi(2)−Te(3)−Bi(2)	87.25(3)
Te(6)−Te(6)−Te(6)	93.25(5)		

[a] Calculated using the cell parameters refined from the powder X-ray diffraction diagram.

(36) Volk, K.; Cordier, G.; Cook, R.; Schäfer, H. *Z. Naturforsch.* **1980**, *35B*, 136−140.

(37) Sutorik, A. C.; Kanatzidis, M. G. *Prog. Inorg. Chem.* **1996**, *43*, 151−265.

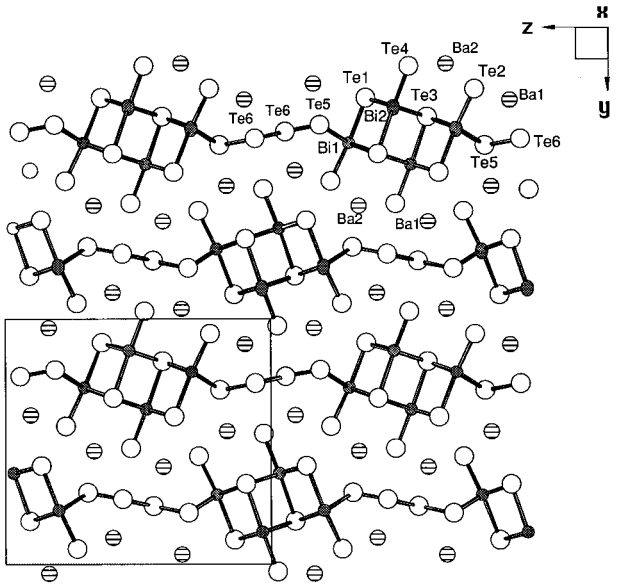

Figure 1. The layered $BaBiTe_3$ structure viewed down the *a*-axis.

(Figure 1) with $[BiTe_3]$ slabs sandwiching Ba cations in pseudo-trigonal prismatic sites. The Ba^{2+} cations occupy sites between layers and are surrounded by nine Te atoms which form a distorted tri-capped trigonal prism. Interestingly, in the coordination polyhedra of both cations one of the capping Te atoms actually caps an edge, while the other two Te atoms cap square faces. There are short distances between Ba^{2+} and the singly-bonded terminal Te(2) and Te(4) atoms in the $[Bi_4Te_{10}]_\infty$ rods at ~3.45 Å, probably due to the stronger Coulombic attraction of the terminal atoms to Ba^{2+}. The remaining Ba−Te distances range from 3.531(2) to 3.887(2) Å. The Coulombic interactions between Ba^{2+} and the nine Te atoms in its coordination polyhedron seem to be important in stabilizing this structure type. We point out that $BaBiTe_3$, $BaBiSe_3$, and $BaSbTe_3$ are all isostructural,[36,38] while the strontium compounds[38,39] are not, probably because a smaller cation such as Sr^{2+} cannot accommodate nine Te atoms in its immediate coordination environment. The size of the alkaline earth metal appears to play an important role in determining the structure type of ternary Group 15 chalcogenide compounds.

The coordination sphere of Bi is best described as distorted octahedral. Each slab contains parallel, rod-shaped columnar $[Bi_4Te_{10}]_\infty$ segments with a NaCl substructure which are made of edge-sharing $BiTe_6$ octahedra. Figure 2 shows different views of one of these segments. The average Bi−Te bond length is 3.196 Å and the average Te−Bi−Te angles (two types) are 89.88° and 172.48°. Although the compound is isomorphous to $BaSbTe_3$,[36] there are notable differences in the degree of structural distortion around the metal atoms from the ideal octahedral motif, with the Sb octahedra being significantly more distorted than those of Bi. This distortion is due to the tendency of the s^2 lone electron pair to stereochemically express itself and is consistent with its greater tendency to do so in Sb than in Bi.

The most notable feature of this structure type is the short Te−Te contacts. The $BaBiTe_3$ contains polytelluride fragments, as can be deduced by assigning a 2+ and a 3+ formal oxidation state to Ba and to Bi, respectively. The average formal oxidation state of Te then is −1.667, raising the expectation for Te−Te bonding. This leads to two possible descriptions of the compound. In the first, the Bi/Te slabs can be thought of as composed of columnar $[Bi_4Te_{10}]_\infty$ segments alternating with parallel "zigzag" Te_n^{n-} "chains" with Te- - -Te contacts (i.e. Te(5)−Te(6) at 3.098(2) Å, see Figure 3a). In the second, the slabs can be thought of as composed of interdigitating columnar $[Bi_4Te_{10}(Te_2)]_\infty$ "herring-bone" shaped segments, according to Figure 3b. Within the would-be zigzag Te_n^{n-} "chains" the Te(6)−Te(6) distance is constant at 3.170(2) Å. The Te(6)−Te(6)−Te(6) angle within the "chain" is 93.25(5)°, similar to that of elemental tellurium but much smaller than the Te−Te−Te angles observed in various $(Te_n)^{2-}$ fragments (around 103°).[40] The Te(5)−Te(6)−Te(6) angle is nearly linear at 170.70(7)°. There is a second type of Te(5)−Te(6) distance between Te atoms in the would-be "zigzag" chain and Te atoms bound to an adjacent $[Bi_4Te_{10}]$ segment at 3.672(2) Å. The latter is comparable to 3.623(4) and 3.728(4) Å of Te−Te distances found between the neighboring Te_3^{2-} anions in the simple Zintl phase $BaTe_3$[23] in which they are not considered bonding. On the other hand, such short contacts were found to be bonding in CdI_2-type polymeric $TiTe_2$ and $IrTe_2$ with a charge transfer from the Te^{2-} sp band to cation d-levels.[41] The bonding situation between the Te atoms in $BaBiTe_3$ is reminiscent of the zig-zag Te chain of $NaBa_6Cu_3Te_{14}$.[42]

While the Te(6)−Te(6) and Te(5)−Te(6) distances are longer than the normal covalent single Te−Te bond length (2.69−2.80 Å),[43] nonetheless, they lie well below the Van der Waals region of 4.0−4.2 Å[44] suggesting possible significant bonding character to them. Because the Te(5)−Te(6) distance is 0.072 Å shorter than the Te(6)−Te(6) distance one is inclined to prefer the interdigitated "herring-bone" description of the structure; however, the Te(6)−Te(6) distances are too short to be ignored from the bonding picture. In order to get a deeper insight into the nature of Te−Te bonding in this region of the structure we carried out electronic band structure calculations.

Description of the Electronic Structure. From a structural point of view, the $[Bi_4Te_{12}]_n^{8n-}$ layers can be divided, as suggested above, into $[Bi_4Te_{10}]$ rods and $[Te_2]$ "chains" linked together via Te(5)−Te(6) interactions. However, the structural data do not allow us to infer a clear view of these interactions. Nevertheless, this model can give a starting point for the description of the electronic structure of the material and a path to clarify the redox competition between these two building blocks. If there is substantial Te−Te bonding within the $[Te_2]$ "chains" then the parameters that will mostly influence the electronic structure and the charge balance will probably be the nature of the Te(5)−Te(6) interactions at the border between the $[Bi_4Te_{10}]$ and $[Te_2]$ building entities.

General Qualitative Electronic Structure Approach. The main aspects of the band structure (for a Bi_4Te_{12} cell content), which can be understood in a very simple way, are the following. A +3 oxidation state has to be assigned to bismuth. Hence its electronic configuration should be $6s^26p^0$ with the two remaining electrons acting as a lone pair (which of course becomes somewhat delocalized through interactions with the nearest neighbors). Moreover, the Bi p orbitals are engaged in highly destabilizing σ^*_{Bi-Te} bonds (right upper part of Figure 4). On

(38) Cook, R.; Schäfer, H. *Studies Inorg. Chem.* **1983**, *3*, 757−760.
(39) Cook, R.; Schäfer, H. *Rev. Chim. Miner.* **1982**, *19*, 19−27.
(40) (a) Böttcher, P. *Angew. Chem., Int. Ed. Engl.* **1988**, *27*, 759−764. (b) Jobic, S.; Brec, R.; Rouxel, J. *J. Alloys Compds.* **1992**, *178*, 253−283.
(41) (a) Canadell, E.; Jobic, S.; Brec, R.; Rouxel, J.; Whangbo, M.-H. *J. Solid State Chem.* **1992**, *89*, 189−199. (b) Jobic, S.; Deniard, P.; Rouxel, J.; Jouanneaux, A.; Fitch, A. N. *Z. Anorg. Allg. Chem.* **1991**, *598/599*, 199−215.
(42) Zhang, X.; Schindler, J. L.; Hogan, T.; Albritton-Thomas, J.; Kannewurf, C. R.; Kanatzidis, M. G. *Angew. Chem., Int. Ed. Engl.* **1995**, *34*, 68−71.
(43) (a) Pauling, L. *Nature of The Chemical Bond*, 3rd rd.; Cornell University Press: Ithaca, NY, 1967; p 246. (b) Burns, R. C.; Gillespie, W. C.; Slim, D. R. *Inorg. Chem.* **1979**, *18*, 3086−3094.
(44) Chauvin, R. *J. Phys. Chem.* **1992**, *96*, 9194−9197.

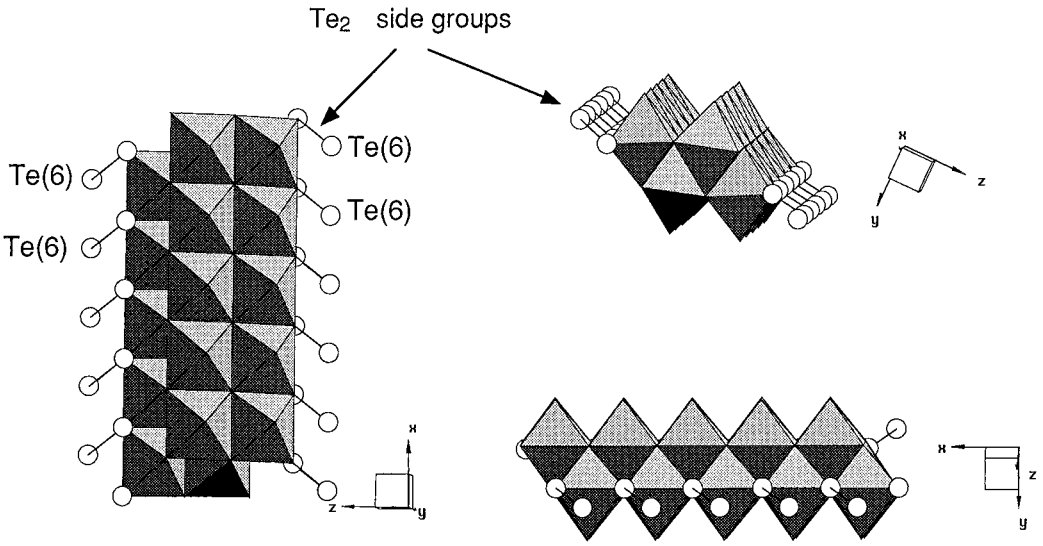

Figure 2. The three views of the columnar $[Bi_4Te_{10}]_\infty$ rod which makes up the structure of the layers in $BaBiTe_3$.

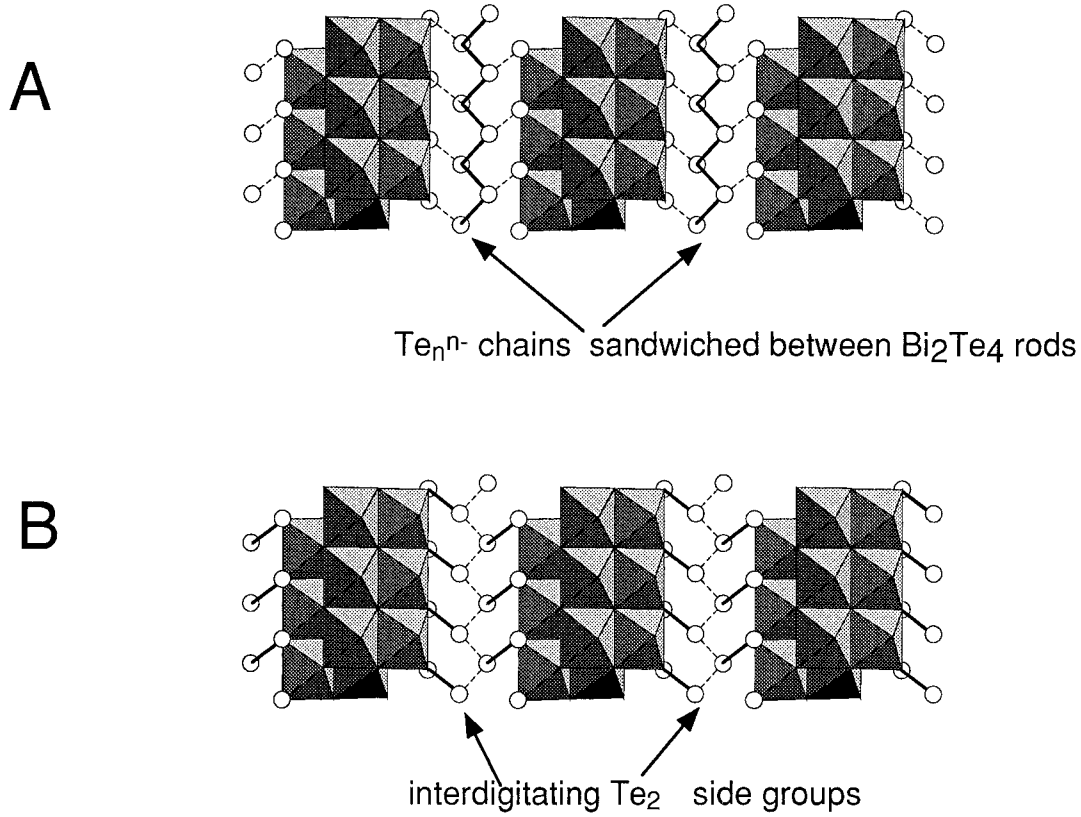

Figure 3. The extended framework of a layer viewed down the *b*-axis showing the two alternative extremes in bonding description regarding the polytelluride part of the structure: (A) $[Bi_4Te_{10}]_\infty$ segments alternating with parallel "zigzag" Te_n^{n-} "chains", (B) interdigitating columnar $[Bi_4Te_{10}(Te_2)]_\infty$ "herring-bone" shaped segments. The barium atoms are omitted for clarity.

the other hand, Te(1), Te(2), Te(3), and Te(4) give rise to a 32 orbital block based on σ_{Bi-Te} bonds and formal "non-interacting" orbitals (left lower part of Figure 4). In view of the great atomic energy level difference between Bi and Te, this 32-orbital block is expected to be much more stabilized as compared to the former two (see Experimental Section above, paragraph on electronic structure calculations).

Now, let us consider the orbitals based on the Te(5) and Te(6) atoms. In a simple model, one Te(5) based orbital is involved in a $\sigma_{Bi(1)-Te(5)}$ bond ($2\sigma_{Bi(1)-Te(5)}$ block), two others are engaged in one σ bond, and one is involved in a $\pi_{Te(5)-Te(6)}$ bond ($2\sigma_{Te(5)-Te(6)}$ and $2\sigma^*_{Te(5)-Te(6)}$ blocks, and 2 orbitals of the 4π orbital block), the last orbital acting as a formal "lone pair" (2 lone pair Te(5) orbital block) (see Figure 4). Also, the four Te(6) orbitals (one s and three p) are engaged as follows: two σ Te(6)−Te(6) bonds (one $\sigma_{Te(6)-Te(6)}$ bonding block, one $\sigma^*_{Te(6)-Te(6)}$ antibonding one), one $\pi_{Te(6)-Te(6)}$ bond (the two remaining orbitals of the 4π orbital block), and the last in σ and σ^* bonds between Te(5) and Te(6). Owing to the long Te−Te distances (Te(6)−Te(6) = 3.170(2) Å, and Te(5)−Te(6) = 3.098(2) Å) as compared to a normal Te−Te single bond (e.g., 2.835(2) Å in elemental Te), the 4π orbitals (based on p_y atomic orbitals) are expected to be located in a narrow energy range and completely filled. In addition, because the Te(5)−Te(6) distances are shorter than the Te(6)−Te(6) distances, the $\sigma^*_{Te(5)-Te(6)}$ bonds are expected to be much more destabilized than the $\sigma^*_{Te(6)-Te(6)}$ bond. Assuming the occurrence of Bi^{3+},

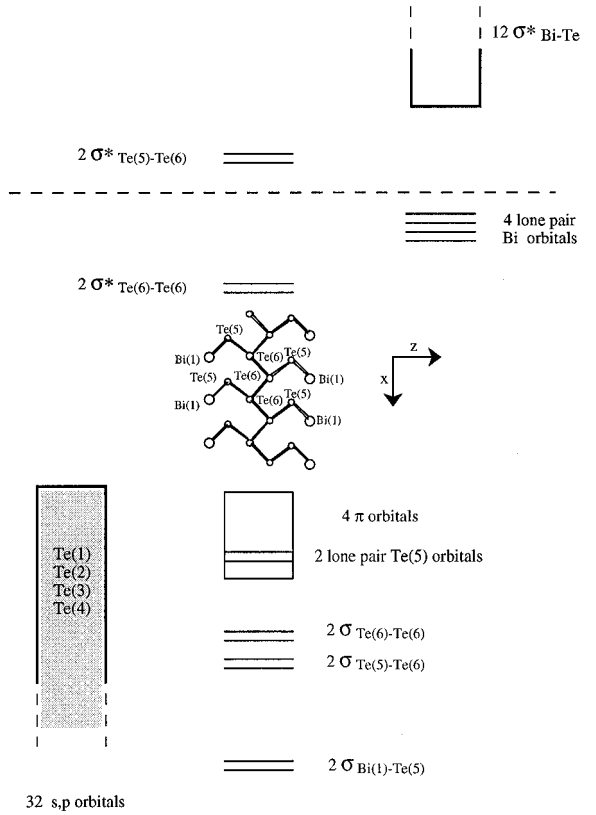

Figure 4. Schematic one-electron energy diagram of a $[Bi_4Te_{12}]_n^{8n-}$ layer. The dotted line represents the expected Fermi level for a $100e^-$ band filling per $[Bi_4Te_{12}]^{8-}$ fragment.

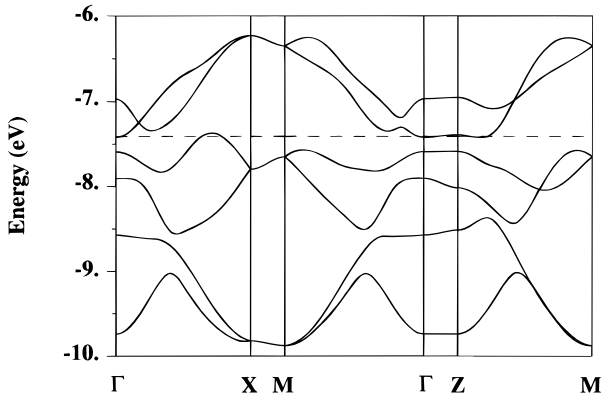

Figure 5. Calculated electronic band dispersion of a $[Bi_4Te_{12}]_n^{8n-}$ layer. The Fermi level is represented by the dashed line. Γ = (0,0,0), X = ($^1/_2$,0,0), Z = (0,0,$^1/_2$), M = ($^1/_2$,0,$^1/_2$).

the four filled lone pairs of Bi have to lie between the two σ antibonding blocks.

Hence we end up with the final band scheme of Figure 4 for a $[Bi_4Te_{12}]_n^{8n-}$ layer. The dotted line represents the expected Fermi level for a $100e^-$ band filling per $[Bi_4Te_{12}]^{8-}$ fragment. A semiconductor behavior is expected if the $\sigma^*_{Te(5)-Te(6)}$ and the Bi lone pair blocks are separated by a gap, but with a strong degree of mixing of the orbitals of the Bi block and those of the Te(5)−Te(6) block, this gap may disappear leading to a metallic behavior. This issue is addressed experimentally below. Notice that in any case the last occupied levels should be essentially based on Bi-s orbitals and the first unoccupied levels on Te(5)−Te(6) based orbitals.

Extended Hückel Calculations. The band dispersion along the high symmetry axis is represented on Figure 5. In the −10 to −6 eV range, six bands are observed, the four lowest based on the so-called Bi lone pairs hybridized with tellurium orbitals,

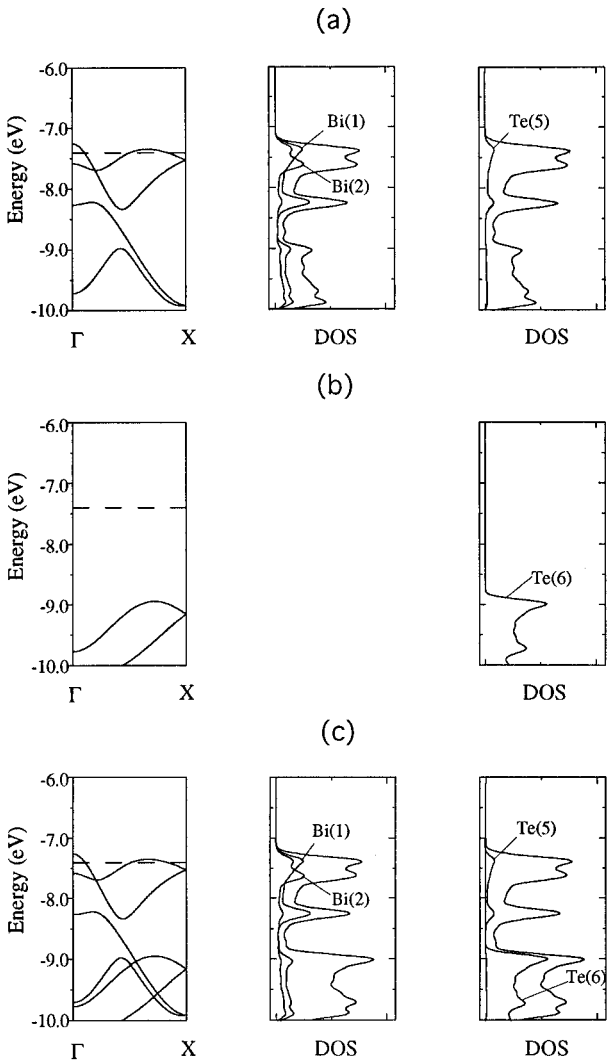

Figure 6. Band dispersion and atomic contribution to the total density of states along Γ−X for the following: (a) an isolated $[Bi_4Te_{10}]$ rod, (b) an isolated $[Te_2]$ "chain", and (c) combined $[Bi_4Te_{10}]$ rods and $[Te_2]$ "chains" with Te(5)−Te(6) distances of 4.810 Å. The dashed line represents the Fermi level calculated for the observed $[Bi_4Te_{12}]_n^{8n-}$ (Te(5)−Te(6), 3.098 Å).

the two highest based on Te(5) and Te(6) orbitals with a slight contribution of the Bi s orbitals. The Fermi level crosses slightly two partially filled bands along the Γ−X axis suggesting a metallic behavior. However, we have to keep in mind that such calculations do not yield accurate band positions and in borderline cases, like the one dealt with here, it is difficult to ascertain the electrical properties of the phase, e.g. metallic or semiconductor.

In order to follow the orbital interactions in going from isolated $[Bi_4Te_{10}]$ rods and $[Te_2]$ "chains" to the real $[Bi_4Te_{12}]_n^{8n-}$ layers, Figures 6 and 7 represent the band dispersion along the common Γ−X direction for different Te(5)−Te(6) distances. The horizontal dotted lines in the figure represent the calculated Fermi level for the $[Bi_4Te_{12}]_n^{8n-}$ structure, and it is used here for comparison purposes only with respect to other energy levels in the diagrams.

The band dispersion calculated for a hypothetical $[Bi_4Te_{10}]$ rod is represented on Figure 6a. The four bands located in the −10 to −7 eV window are based on Bi s atomic orbitals (the Te-based s, p band is found below −12.6 eV and is not represented on the picture). Therefore, the Bi-based and Te-based contributions are well separated. Figure 6b shows the band dispersion for a hypothetical isolated $^1_\infty[Te_2]$ "chain". All

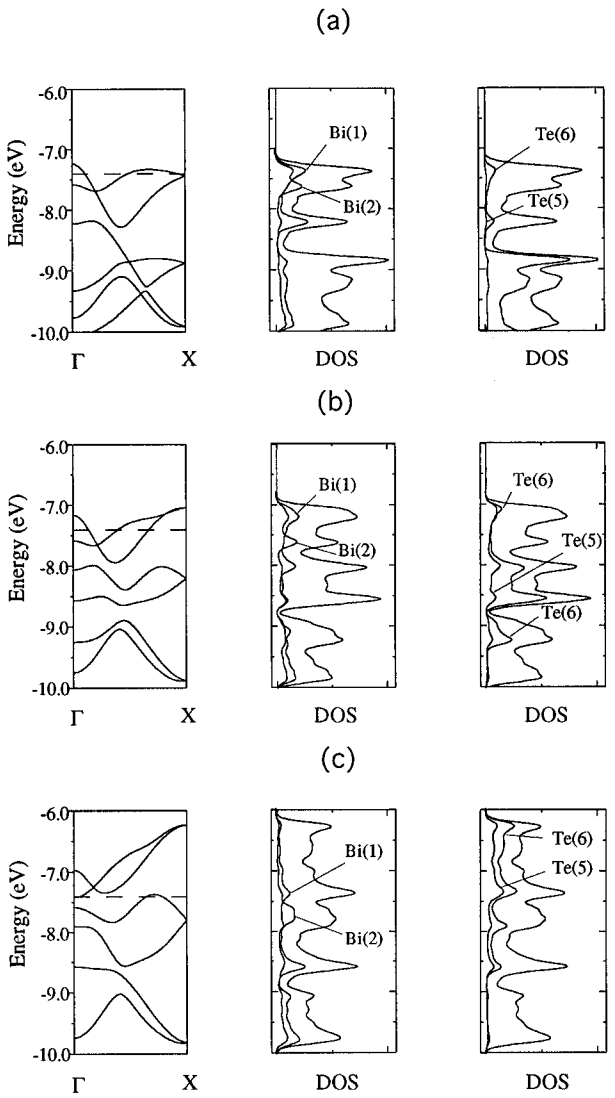

Figure 7. Band dispersion and atomic contribution to the total density of states along Γ−X for the following: (a) same as Figure 6c but with Te(5)−Te(6) distances of 3.697 Å, (b) same as Figure 6c but with Te(5)−Te(6) distances of 3.279 Å, (c) same as Figure 6c but with Te(5)−Te(6) distances of 3.098 Å. The dashed line represents the Fermi level calculated for the observed $[Bi_4Te_{12}]_n^{8n-}$ (Te(5)−Te(6), 3.098 Å).

the bands (eight) lie between −9 and −22.4 eV (only the two upper ones are represented). Therefore, as the $[Bi_4Te_{10}]_n$ and $[Te_2]$ entities approach each other side by side one would expect electron transfer from the Bi s-based band to the Te(6) s, p-based band.

As we decrease the Te(5)−Te(6) distance, we observe a shift to higher energy via some hybridization between the Te(5)- and Bi-based bands and the Te(6)-based bands (Figure 6c to Figure 7c). The evolution of the atomic contributions of Bi(1), Bi(2), Te(5), and Te(6) to the total density of states along the Γ−X axis, as the bands disperse with decreasing distance between the $[Bi_4Te_{10}]_n$ rods and $[Te_2]$ "chains", is illustrated in Figure 6 and 7. As the one-dimensinonal infinite fragments get closer, the energy of the two bands based on Te(6) atoms increases to levels higher than those made of Bi lone pairs. Moreover, a Mulliken population analysis performed on a hypothetical infinite $[Bi_4Te_{10}]_n^{8n-}$ rod and a $[Bi_4Te_{12}]_n^{8n-}$ layer confirms this trend (Table 6). Going from the rod (with formally Te^{2-} anions) to the layer, we notice a considerable decrease of the electronic population on Te(5) with a concomitant increase of the population on Bi(1). The other atomic sites (Bi(2), Te(1), Te(2), Te(3), and Te(4)) seem insensitive to the decreasing distance

Table 6. Mulliken Gross Population and Net Atomic Charge in $[Bi_4Te_{10}]_n^{8n-}$ Rod and $[Bi_4Te_{12}]_n^{8n-}$ Layer

	gross population		net atomic charge		
	$[Bi_4Te_{10}]_n^{8n-}$ rod	$[Bi_4Te_{12}]_n^{8n-}$ layer	$[Bi_4Te_{10}]_n^{8n-}$ rod	$[Bi_4Te_{12}]_n^{8n-}$ layer	Δ
Bi(1)	3.27	3.05	+1.73	+1.95	0.22
Bi(2)	3.25	3.17	+1.75	+1.83	0.08
Te(1)	7.32	7.26	−1.32	−1.26	0.06
Te(2)	7.64	7.60	−1.64	−1.60	0.04
Te(3)	7.22	7.11	−1.22	−1.11	0.11
Te(4)	7.63	7.61	−1.62	−1.61	0.01
Te(5)	7.67	7.16	−1.67	−1.16	0.51
Te(6)		7.04		−1.04	

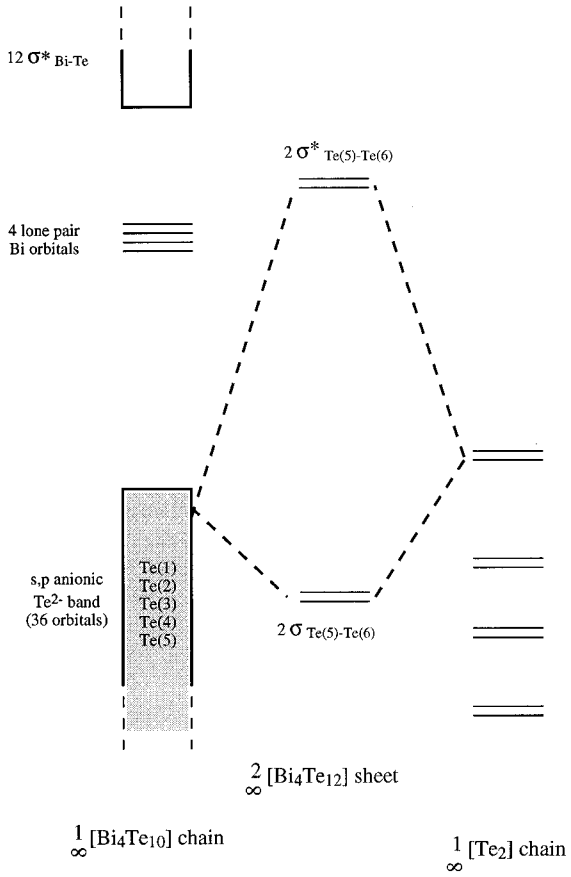

Figure 8. Schematic band diagram illustrating the influence of a decreasing Te(5)−Te(6) distance on the Te(5)−Te(6) σ orbital energy levels.

between the Te(5) and the Te(6) atoms, because they are too far away from the interface between the $[Bi_4Te_{10}]_n$ rods and the $[Te_2]$ "chains". Figure 8 sums up the interactions which take place when the fragments get closer. The higher contribution of Te(6) to the $\sigma^*_{Te(5)-Te(6)}$ block originates from the fact that Te(5) is more stabilized in energy in view of its direct interaction with the Bi cation (polarization effect) and by consequence contributes more to the bonding $\sigma_{Te(5)-Te(6)}$ bonds than to the $\sigma^*_{Te(5)-Te(6)}$ ones. The proposed charge balance, not taking into account the slight hybridization of Bi(1) with Te(5) and Te(6), is $Ba^{2+}{}_4Bi^{3+}{}_4Te^{2-}{}_8Te^{1-}{}_4$. We note that the integrated calculated overlap population (e^-/bond) at the Fermi level for the Te(5)−Te(6) (3.098(2) Å) and Te(6)−Te(6) (3.170(2) Å) bonds are 0.051 and −0.032, respectively. The Te(5)−Te(6) interactions are bonding in character, while the Te(6)−Te(6) contacts are antibonding. The Te(5)−Te(6) bond qualitatively resembles the bond found in isolated $(Te_2)^{2-}$ pairs, but differs quantitatively since the Te(6) atoms are perturbed by the contact of neighboring $[Bi_4Te_{12}]$ blocks. On the other

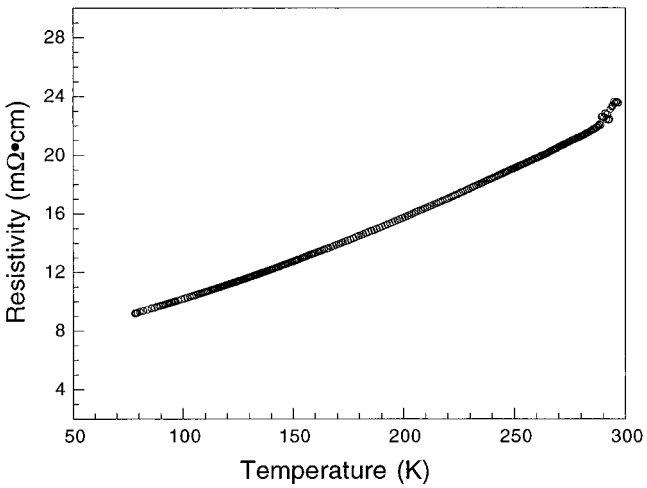

Figure 9. Variable-temperature electrical resistivity data for single crystals of p-type $BaBiTe_3$.

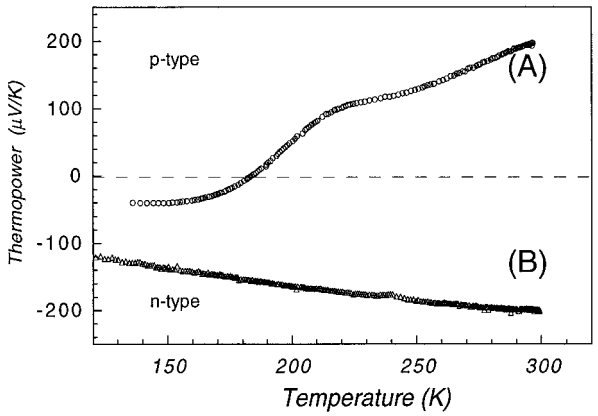

Figure 10. Variable-temperature thermoelectric power data for (A) p-type and (B) n-type $BaBiTe_3$.

hand, the overall negative overlap population between Te(6)−Te(6) rules out the occurrence of a $[Te_2]_n$ "chain", and the Bi−Te layers in this compound should be thought of as formed by the zipper-like interaction of interdigitating $[Bi_4Te_{12}]_n^{8n-}$ blocks (see Figure 3). It can thus be said that there is no $[Te_2]_\infty$ "chain" in $BaBiTe_3$. The particular Te···Te short contact is to be seen as the result of a particular sphere packing required by the structure to accommodate successive $[Bi_4Te_{12}]_n^{8n-}$ ribbons. This explains (see below) why the Te(6)−Te(6)−Te(6) angle is so different from the expected angles for a chain.

Charge Transport Properties. The nature of the electronic band structure suggests strongly that the material will have interesting charge transport properties. The electrical properties of $BaBiTe_3$ were measured from single crystal samples. The conductivity at room temperature was found between 20 and 50 S/cm with a weak negative temperature coefficient consistent with a metal-like or semimetallic material, see Figure 9. Qualitatively, the temperature dependence is similar to that of Bi_2Te_3.[1c,45] The nature of the carriers was probed with thermoelectric power measurements as a function of temperature. We find it interesting that we can obtain both n-type and p-type samples of this material based on the preparation method. The n-type material forms from Te-rich cesium polytelluride flux, and the p-type forms from potassium polytelluride flux. In Cs_2Te_x flux Te substitution of Bi atoms could account for the n-type nature of the material. Given the similar size of K^+ and Ba^{2+}, one may speculate that in K_2Te_x flux some substitution of Ba^{2+} by K^+ atoms renders the compound p-type by creating holes in the valence band. In both cases the room temperature Seebeck coefficient is quite large, ∼−200 and ∼+200 μV/K, respectively, see Figure 10. These values decrease and tend toward zero at lower temperatures. The p-type samples exhibit a kink of unknown origin at ∼215 K and an unusual sign reversal below 185 K. The sign reversal to negative values is smooth and continuous as the data cross through zero and suggests that electrons at low temperatures are either more numerous or more mobile than holes. This behavior is not observed in the n-type samples where the Seebeck coefficient decreases but remains negative. Undoubtedly, the thermopower data reflect the substantial complexity of the electronic band structure at the Fermi level of this material, as is suggested by the band structure calculations. Certainly, the band structure in Figure 5 is consistent with the simultaneous occurrence of holes and electrons as carriers. Despite the metal-like temperature dependence of the electrical conductivity and thermopower one cannot unequivocally conclude that $BaBiTe_3$ is a metal since the magnitude of the Seebeck coefficients is too large for a typical metal. The overall behavior is similar to the parent binary phase Bi_2Te_3, albeit the ternary derivative has a lower electrical conductivity. Therefore, at this stage neither the extended Hückel electronic structure calculations nor the charge transport measurements are sufficient to distinguish between a truly metallic behavior from a semimetallic or narrow gap semiconductor behavior. Further work is needed to unequivocally address this issue, see below.

Model for the Transport Properties and Existence of Energy Gap at E_F. As previously mentioned, the extended Hückel calculations suggest the occurrence of a metallic behavior with a poor conductivity in relation with a low density of states at the Fermi level. This agrees qualitatively with the observed electrical conductivity of the material; however, the magnitude of conductivity is too low for a normal metal and closer to that of a semi-metal of a narrow-gap semiconductor, similar in nature to the semiconductor Bi_2Te_3. However, a metal-like model does not explain (1) the magnitude of the thermoelectric power with the temperature and (2) the different nature of the charge carrier according to the crystal preparation route. For these reasons, self-consistent *ab initio* band structure calculations within the TB-LMTO-ASA method[46,47] were undertaken to predict with more accuracy the electronic behavior of the compound. All the atoms were taken into account.

In contrast to the extended Hückel calculations, which are not suitable for the estimation of band gaps, the more rigorous TB-LMTO-ASA calculations[48] suggest an opening of a small indirect gap (0.3 eV) between the so-called bismuth lone pair block and the $\sigma^*_{Te(5)-Te(6)}$ block leading to a semiconductor-type behavior. Notice that this calculation method is known to underestimate the band gap. This model is more consistent with the measured transport properties. In the 70−300 K temperature range, the "exhaustion regime" might be reached (in a narrow

(45) Buist, R. J. *CRC Handbook of Thermoelectrics*; Rowe, D. M., Eds.; CRC Press, Inc.: Boca Raton, FL, 1995; p 143.

(46) Andersen, O. K.; Jepsen, O. *Phys. Rev. Lett.* **1984**, *53*, 2571−2574 and references therein.

(47) Krier, G.; Jepsen, O.; Burkhardt, A.; Andersen, O. K. *The TB-LMTO-ASA program*, version 45; Max-Planck-Institut Für Festkörperforschung: Heisenbergstrasse 1, D-70569 Stuttgart, Germany.

(48) (a) Exchange and correlation were treated in the local spin density approximation. All the relativistic effects except spin−orbit coupling were taken into account using the scalar relativistic approximation. Since the structure of the present compound is not closely packed, special care was taken in filling the interatomic spaces with interstitial spheres (ES). Optimal positions and radii of those empty spheres were determined by the automatic procedure described in ref 48b. The *k*-space integration was performed with the tetrahedron method and the charge self-consistency was obtained with 801 irreducible *k*-points. (b) Jepsen O.; Andersen O. K. *Z. Phys. B* **1995**, *97*, 35−47.

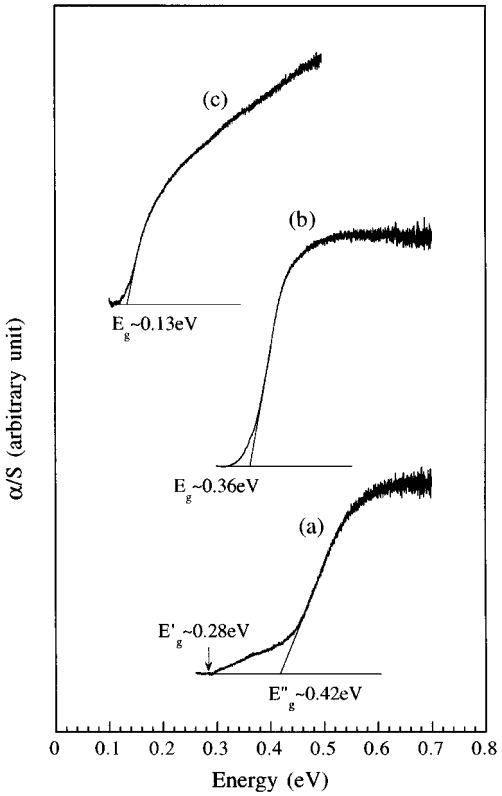

Figure 11. A comparison of infrared absorption spectra of (a) $BaBiTe_3$, (b) PbS, and (c) Bi_2Te_3. The semiconductor energy gaps are indicated in the spectra.

gap semiconductor) explaining the metal-like properties with a low conductivity. According to the temperature, the different nature of the charge carriers could originate from the differential depopulation of the valence and conduction bands and from the greatly differing mobilities of the holes and electrons. At low temperatures hole localization may leave electrons as the only carriers and to n-type conductivity. That the materials can be doped both n- and p-type implies the occurrence of donor and acceptor levels in the gap. The acceptor levels may be based on a slight excess of Bi situated on Te sites, while the donor levels would suggest the occurrence of a slight excess of Te on Bi sites. Such a non-stoichiometry is common among heavy chalcogenides and should be probed further because it could permit the tuning of the properties of $BaBiTe_3$ and the achievement of good thermoelectric performance. The key property to be improved is the magnitude of the electrical conductivity, since the thermal conductivity is already very low, see below.

To experimentally address the important issue of whether the compound is a metal or a semiconductor we performed optical measurements over a wide range of wavelengths. The technique of diffuse reflectance spectroscopy in the infrared range is well suited for the determination of band gaps in narrow band semiconductors. The use of known materials with gaps in the same range as standards confirmed the reliability of the measurements. With PbS, PbSe, and Bi_2Te_3 as standards at room temperature we obtained gaps of 0.36, 0.26, and 0.13 eV, respectively, in excellent agreement with the literature values of 0.37, 0.26, and 0.15 eV,[49] see Figure 11. Diffuse reflectance

(49) (a) Pankove, J. I. *Optical Process in Semiconductors*; Dover Publications, Inc.: New York, 1971; p 413. (b) Encyclopedia of Materials Science and Engineering, *Thermoelectric Semiconductors*; MIT Press: Cambridge, MA; Pergamon Press: Oxford, 1986; p 4968. (c) Li, C. Y.; Ruoff, A. L.; Spencer, C. W. *J. Appl. Phys.* **1961**, *32*, 1733. (d) Austin, I. G. *Proc. Phys. Soc.* **1958**, *72*, 545.

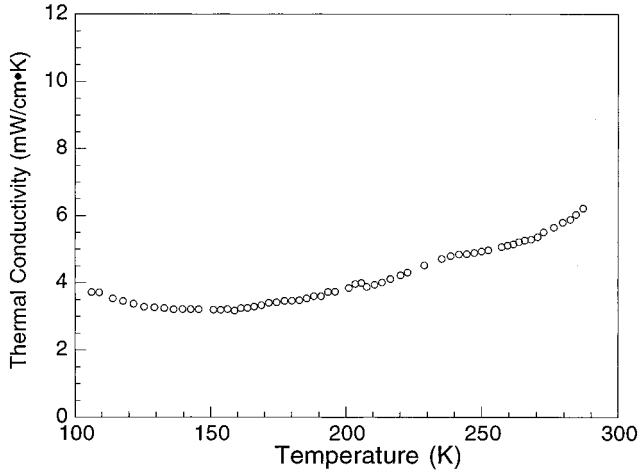

Figure 12. Variable-temperature thermal conductivity data for single crystals of p-type $BaBiTe_3$.

spectroscopy on $BaBiTe_3$ at room temperature revealed the presence of absorptions which can be assigned to a band-gap. Two closely spaced absorptions at 0.28 and 0.42 eV are observed and the shallow slope of the lowest energy transition is consistent with the LMTO calculations which predict a narrow indirect gap. The transition at 0.42 eV could be assigned to excitations between other more widely spaced bands.

Thermal Conductivity. Thermoelectric applications demand a very low thermal conductivity in the temperature range of interest. Therefore, the thermal conductivity of $BaBiTe_3$ was measured as a function of temperature, Figure 12. The data show a remarkably low thermal conductivity with respect to that of Bi_2Te_3 (κ_L ~1.6 W/(m·K)).[49b] Using the measured values of the electrical resistivity in conjunction with the Wiedemann−Franz law,[50] we estimate the maximum possible value of the electronic thermal conductivity contribution to be below 1% of the total thermal conductivity of $BaBiTe_3$. Thus, essentially all heat in the compound is carried by lattice phonons. Hence, at least from the perspective of thermal transport, the $BaBiTe_3$ satisfies one of the key requirements for a useful thermoelectric material, and in fact, it possesses one of the lowest thermal conductivity values ever reported for a potential thermoelectric material. The very low thermal conductivity of $BaBiTe_3$ implies that the modification of the structure and composition of Bi_2Te_3 by the incorporation of $BaTe_x$ or A_2Te_x into it is a correct approach in lowering its lattice thermal conductivity. The calculated zT at room temperature using σ = 42 S/cm, S = 205 μV/K, and κ = 6.3 mW/(cm·K) is 0.085 compared to ~0.9 for Bi_2Te_3. If ways could be found to enhance the electrical conductivity and, at the same time, preserve or even increase the already large thermopower a promising thermoelectric material might be obtained. To achieve this we need additional information regarding the transport properties including carrier concentrations and mobilities. Then optimization of these properties could be accomplished by controlling accurately the stoichiometry of these materials. This work is currently underway.

Concluding Remarks

Our studies of structure and bonding in $BaBiTe_3$ show that there are no zigzag Te "chains" in this material. Rather, the compound is better described as one-dimensional in which infinite $[Bi_4Te_{12}]_n^{8n-}$ rods assemble side-by-side into layers leading to interdigitating $(Te^{1-})_2$ side groups. $BaBiTe_3$ is a

(50) Kittel, C. *Introduction to Solid State Physics*, 6th ed.; John Wiley & Sons, Inc.: New York, 1986; p 150.

narrow gap semiconductor with probably an indirect gap and it possesses a very low lattice thermal conductivity which makes it attractive for further studies as a thermoelectric material. If the crystal quality can be improved and the level of dopants controlled, significant increases in electrical conductivity could be expected without losses in thermopower. This work suggests that this is possible by K doping in Ba sites (p-type) and Te doping of Bi sites (n-type). This could greatly increase the potential thermoelectric performance of this material. The elaborate electronic structure of $BaBiTe_3$ at the Fermi level is responsible for the large values of thermoelectric power. It suggests that large changes could be observed in the thermoelectric properties of this material with the application of a relatively small amount of pressure. It would be interesting to see how the material reacts to pressure.

Acknowledgment. Financial support from the Office of Naval Research (Contract No. N00014-94-1-0935, M.G.K. and C.R.K.) is gratefully acknowledged. The work made use of the SEM facilities of the Center for Electron Optics at Michigan State University. At NU this work made use of Central Facilities supported by NSF through the Materials Research Center (DMR-96-32472). M.G.K. thanks the "Pays de la Loire" region for support during a sabbatical stay in Nantes, 1996.

Supporting Information Available: Tables of crystallographic data and anisotropic thermal parameters of all atoms (2 pages). See any current masthead page for ordering and Internet access instructions.

JA9636496